Variable-Bandwidth Superchannels Using Synchronized Colorless Transceivers

Milad Sharif and Joseph M. Kahn, *Fellow, IEEE*

***Abstract*—We propose a modular architecture for long-haul optical networks supporting flexible-bandwidth superchannels. Colorless transceivers can be designed to modulate/detect up to $M = 4$ subcarriers, each at a symbol rate of 12.5 Gbaud, achieving a maximum bit rate of 200 Gbit/s, assuming polarization-multiplexed quadrature phase-shift keying (PM-QPSK). A set of N synchronized transceivers can cooperate to modulate/detect a superchannel comprising $N{\cdot}M$ subcarriers using no-guard-interval orthogonal frequency-division multiplexing, enabling transmission at bit rates beyond 1 Tbit/s. We analyze and simulate the performance of the proposed architecture in the presence of linear fiber impairments and synchronization errors and establish design requirements for practical deployment of the architecture. Simulation results are shown for transmission of a superchannel comprising 24 subcarriers, which conveys approximately 1.1 Tbit/s with a spectral efficiency of 3.5 bits/s/Hz using PM-QPSK.**

***Index Terms*—Communication system performance, flexible bandwidth, long-haul systems, multi-carrier optical systems, no-guard-interval (NGI) orthogonal frequency-division multiplexing (OFDM), superchannels, terabit channels, variable-bandwidth channels.**

I. Introduction

OPTICAL superchannels have attracted significant interest as a means for increasing spectral efficiency and per-channel bit rates. Multiple constituent channels originating at a common node are multiplexed with little or no guard interval to form a superchannel, which is routed through a network as a single entity. Superchannels avoid optoelectronic and electronic speed limitations via optical parallelism and increase spectral efficiency by efficient use of the optical spectrum. Several techniques have been demonstrated for transmission of superchannels using either single-carrier (SC) modulation or orthogonal frequency-division multiplexing (OFDM).

In no-guard-interval (NGI) coherent optical OFDM, also referred to as all-optical OFDM [1]–[4], multiple SC-modulated subcarriers are multiplexed with a frequency spacing exactly equal to the symbol rate. Constituent subcarriers require precise symbol and carrier phase synchronization in order to be mutually orthogonal in the absence of dispersion. Digital equalization with at least 4 samples per symbol is required to compensate for inter-symbol interference (ISI) and inter-channel interference (ICI) caused by dispersion [2].

In Nyquist WDM [5], [6], SC-modulated constituent channels are spectrally shaped to make them bandlimited, and are multiplexed with a frequency spacing slightly higher than the symbol rate to form a superchannel. In Nyquist WDM, constituent channels require tight pre-filtering, performed either digitally or optically at the transmitter, to avoid ICI. ISI caused by dispersion can be removed through digital equalization at the receiver.

Theoretical and experimental comparisons of these two approaches can be found in [7], [8]. As compared to NGI-OFDM, Nyquist WDM achieves lower spectral efficiency, but has more relaxed requirements on receiver bandwidth and ADC sampling rate and avoids the need for precise frequency/symbol rate synchronization between subcarriers.

Alternatively, constituent channels can be modulated by OFDM generated digitally using the inverse discrete Fourier transform (DFT) [9], [10]. In order to overcome ISI and ICI, a sufficiently long cyclic prefix is required, which reduces spectral efficiency. An architecture for bandwidth-scalable and colorless superchannel transmission using DFT-based OFDM was proposed in [11]. However, DFT-based OFDM is known to be less tolerant to fiber nonlinearity than SC modulation, since collections of many subcarriers are coherent over a long symbol period and efficiently generate four-wave mixing products [12].

Most previous studies of NGI-OFDM modulated superchannels using dedicated transmitters designed for a fixed bandwidth and wavelength. In dynamic optical networks, such dedicated transmitters might frequently be significantly underutilized. Only a few studies [11], [13] addressed the scalability and wavelength agility of superchannels, which is essential for efficient elastic optical networking. In [13], authors experimentally demonstrated a colorless flexible signal generator based on a reconfigurable optical switch, but did not address synchronization requirements for practical superchannel systems.

In this paper, we propose a system architecture enabling NGI-OFDM superchannels that are wavelength-agile, and whose bit rates can scale with traffic demands. Transceivers are colorless and operate at aggregate symbol rates up to 50 Gbaud, conveying approximately 180 Gbit/s (assuming 7% FEC overhead). Each transmitter can operate independently, or multiple transceivers can cooperate to transmit a superchannel with a bit rate beyond 1 Tbit/s. Cooperation of multiple transceivers avoids the need for dedicated transceivers that can (de)modulate entire superchannels. In this paper, we establish design and synchronization requirements for such a colorless, bandwidth-scalable system.

The remainder of this paper is organized as follows. In Section II, we describe the variable-bandwidth network

Manuscript received December 16, 2013; revised January 28, 2014; accepted February 23, 2014. Date of publication March 13, 2014; date of current version May 7, 2014. This work was supported by a Google Research Award.

The authors are with the E. L. Ginzton Laboratory, Department of Electrical Engineering, Stanford University, Stanford, CA 94305 USA (e-mail: msharif@stanford.edu; jmk@ee.stanford.edu).

Color versions of one or more of the figures in this paper are available online at http://ieeexplore.ieee.org.

Digital Object Identifier 10.1109/JLT.2014.2310692

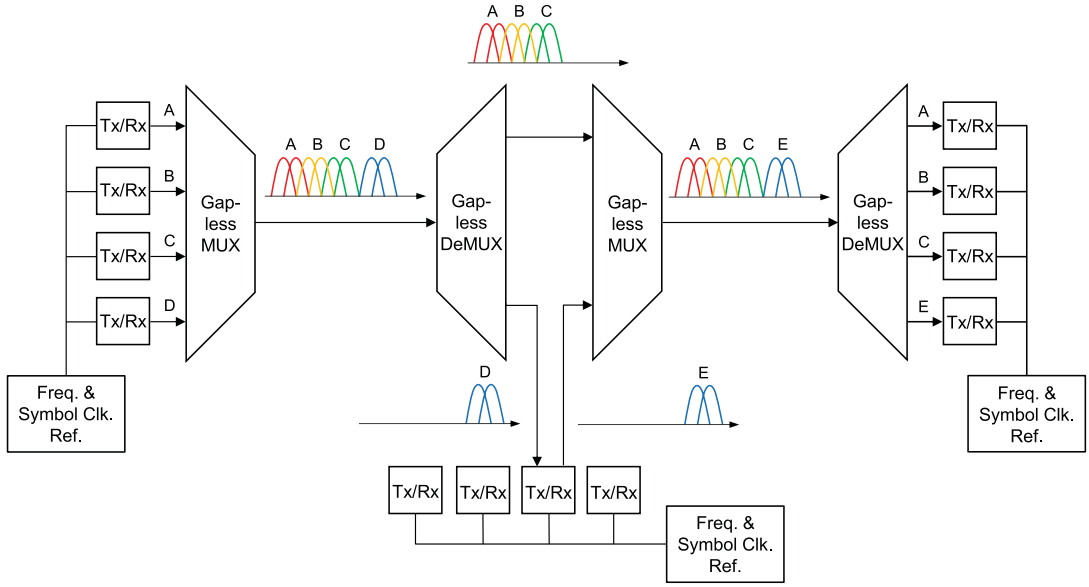

Fig. 1. Optical network with variable-bandwidth superchannels.

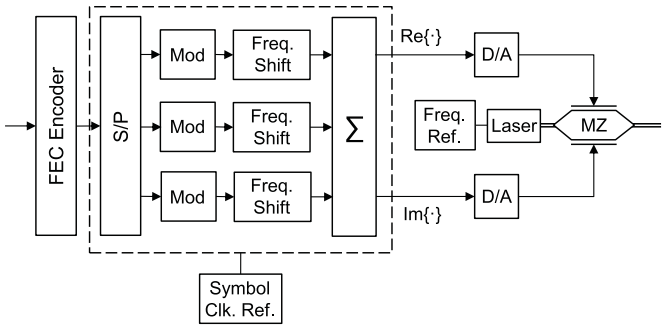

Fig. 2. Block diagram of a transceiver generating $M = 3$ subcarriers (only one polarization is shown).

architecture and its necessary components. In Section III, we explain requirements for sampling and digital signal processing at the receiver side. We analyze the performance of the proposed system in the presence of various impairments and synchronization errors. We present conclusions in Section V.

II. Variable-Bandwidth Superchannels

A. Colorless Transceivers and Synchronization

Fig. 1 shows an exemplary transmission system using variable-bandwidth superchannels. Each transceiver can be tuned to (de)modulate a block of M_{Tx} subcarriers on any wavelength within a desired band and collection of N transceivers can cooperate to (de)modulate a superchannel with $N{\cdot}M_{Tx}$ subcarriers. The maximum number of subcarriers within a block is limited by the sampling rate of the ADC and the bandwidth of the optoelectronic components. In this paper we consider blocks with up to $M_{Tx} = 4$ subcarriers due to these practical constraints.

A transmitter generating $M_{Tx} = 3$ subcarriers is shown schematically in Fig. 2. Encoded symbols are modulated using M_{Tx} modulators in parallel. Real and imaginary components of the sum of frequency-shifted subcarriers are used to drive the MZ modulator. Pre-distortion and frequency-response compensation can be used in the transceiver to mitigate the impact of modulator nonlinearity and frequency-dependent electrode losses on the system performance [14].

In order to minimize crosstalk between subcarriers modulated by different transceivers, the carrier frequencies and symbol clocks of the transceivers need to be synchronized. These are locked to a frequency comb and symbol clock reference that is broadcast to all the transceivers [15]. The frequency comb is not demultiplexed into separate carriers to be individually modulated, which is the key to enabling colorless superchannel generation. The same oscillator is used for the symbol clock and frequency comb references, so the symbol rate is precisely matched to the subcarrier spacing.

B. Colorless Gapless (De)Multiplexing

The variable-bandwidth network shown in Fig. 1 requires wavelength-selective switches (WSSs) that can add/drop superchannels consisting of N blocks to/from N ports without spectral gaps, and can also pass through (express) an arbitrarily wide superchannel. Possible realizations of such colorless gapless demultiplexing are shown in Fig. 3. In one approach, as shown in Fig. 3(a), superchannel is split in to N copies using a conventional liquid crystal-on-silicon (LCOS) WSS in combination with a star coupler. Power splitting could alternatively be achieved by directing the beam to N drop ports [16]. In any case, splitting the superchannel among N ports leads to loss of $1/N$, which increases with N.

In a second approach, shown in Fig. 3(b), a dual-mode WSS splits a portion of the superchannel spectrum equally to three contiguous ports [11]. This leads to a loss of 1/3 (-4.8 dB) independent of N, which is more efficient than N-way splitting when $N > 3$. However, this design is not suitable for variable-bandwidth networks with $M = 1$, since the bandwidth

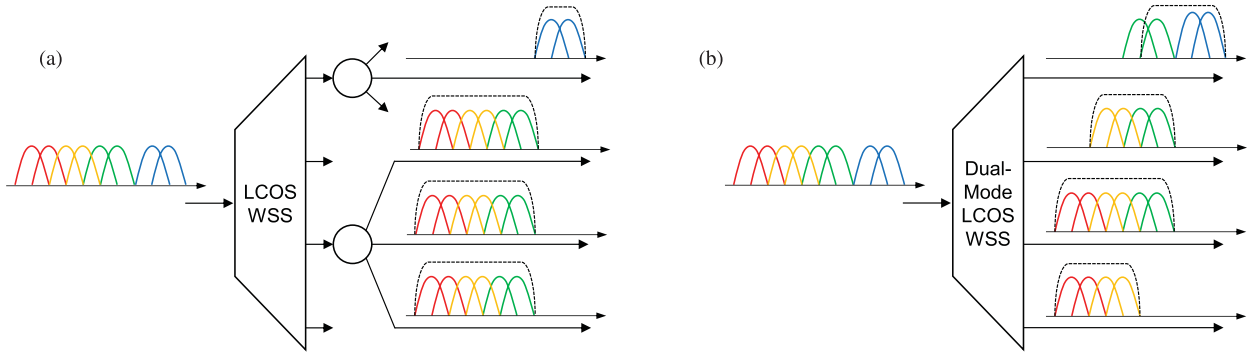

Fig. 3. Possible realizations of colorless gapless demultiplexer at the rightmost node of Fig. 1 using: (a) conventional WSS with star coupler and (b) dual-mode WSS. WSS passbands and central lobes of signal spectra are represented by dashed and solid lines, respectively.

of the passband of the add/drop ports becomes smaller than the required receiver bandwidth, and ICI from adjacent subcarriers cannot be suppressed. Further details of the receiver bandwidth requirements are given in Section III. As compared to N-way splitting, the dual-mode WSS requires a larger number of add/drop modules to support a given bandwidth, assuming a fixed number of add/drop ports per module.

It is worth noting that because of the variable bandwidth of the superchannels, their center frequencies may not coincide with the standard 50-GHz ITU grid. Hence, it is necessary that the (de)multiplexers be compatible with the recent ITU-standard flexible grid supporting center-frequency and bandwidth granularities of 6.25 and 12.5 GHz [17].

C. Detecting Multiple Subcarriers Per Sampling

At the destination node, copies of the superchannel or a portion of it, depending on the demultiplexer implementation, appear at multiple output ports of the demultiplexer. The desired subcarrier is generally accompanied by adjacent subcarriers, which overlap the desired subcarrier, and cannot be separated by optical filtering without incurring a penalty. In order to separate the subcarriers effectively, the sampling rate $R_{\rm samp}$ should be high enough that the Nyquist bandwidth defined by $|f-f_{LO}| < R_{\rm samp}/2$ includes the desired subcarrier and any neighbors overlapping it. The cost and complexity of the wideband receiver and high sampling rate can be amortized by simultaneous detection of M_{Rx} subcarriers per digital sampling. However, as shown in Fig. 4, as M_{Rx} increases, the Nyquist bandwidth may not be sufficient to include the interfering neighbors, resulting in a performance penalty. Penalties for detection of $M_{Rx} \leq 3$ subcarriers were evaluated experimentally in [18], and are studied in Section III-B for $M_{Rx} \leq 4$.

In practice, it is typically desired that each transceiver transmit and receive an equal number of subcarriers. Hence, for the remainder of the paper, we assume $M_{Rx} = M_{Tx} = M$.

III. System Design Requirements

In this section, we study key requirements for enabling several transceivers to cooperate in (de)modulating a variable-bandwidth superchannel. We define a receiver digital signal processing architecture and study the impact of the number

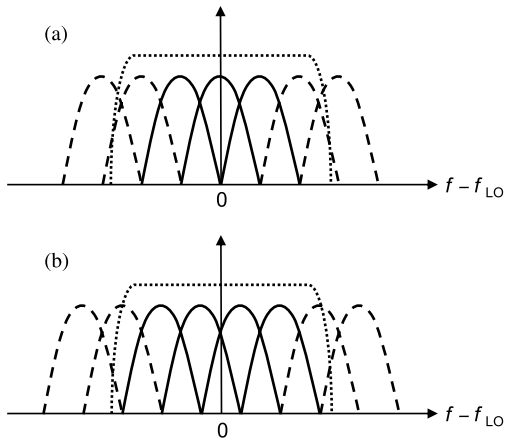

Fig. 4. Frequency spectra for detection of (a) $M = 3$ and (b) $M = 4$ subcarriers per sampling for $R_s = 12.5$ GHz and sampling rate of 75 GHz. The Nyquist bandwidth corresponding to $|f-f_{LO}| < R_{\rm samp}/2$ is represented by dotted lines. The central spectral lobes of the desired and interfering subcarriers are represented by solid and dashed lines, respectively.

of subcarriers detected per sampling. We study the impact of transceiver synchronization errors, enabling us to specify synchronization requirements. We consider $M = 1, 2, 3, 4$ subcarriers per transceiver.

A. Receiver Digital Signal Processing

Fig. 5 shows detection of $M = 2$ subcarriers per sampling. First, chromatic dispersion compensation is performed using overlap frequency-domain equalization (FDE) [19], which avoids the need for a time-domain guard interval. Subsequently, each subcarrier is frequency-shifted to baseband and passed through a subcarrier separation filter, which is essentially a matched filter for a single subcarrier. The subcarrier separation filter can be implemented either in the time domain by cascading delay-and-add filters or in the frequency domain. In both our analysis and simulation, we use a frequency-domain sinc function, which is an ideal matched filter [7].

Adaptive equalization is then employed to compensate polarization mode dispersion and the residual chromatic dispersion. We consider adaptive equalization without use of training sequences. In the first step, we employ the constant modulus algorithm (CMA) which minimizes the distance of the equalized

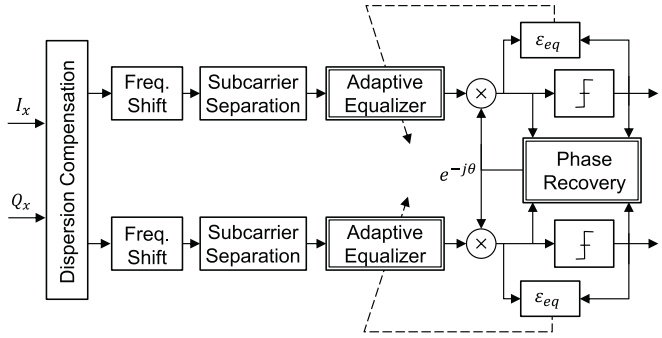

Fig. 5. Detection of two subcarriers per sampling employing adaptive equalization and joint carrier phase recovery (only one polarization is shown). Equalization and phase recovery are done jointly for two polarizations.

symbols from a circle of constant radius. The CMA cost function is given by

$$\varepsilon_{\mathrm{CMA}} = 1 - |x_{\mathrm{out}}(n)|^2 \tag{1}$$

where $x_{\mathrm{out}}(n)$ is the nth equalized symbol and the adaptive filter coefficients are updated according to

$$h \rightarrow h + \mu \varepsilon_{\mathrm{CMA}} x_{\mathrm{in}}(n) x_{\mathrm{out}}^{*}(n) \tag{2}$$

where μ is a convergence parameter and x_{in} is the received symbol. The CMA cost function is independent of the carrier phase, which decouples equalization and carrier phase recovery. However, as shown in [20], decision-directed least mean squared (LMS) has better performance. Therefore, after pre-convergence is obtained using CMA, we switch the filter adaptation to the decision-directed mode and use LMS cost function and filter update, which are given by

$$\begin{aligned} \varepsilon_{\mathrm{LMS}} &= d(n) - e^{-j\phi} x_{\mathrm{out}}(n) \\ h &\rightarrow h + \mu \varepsilon_{\mathrm{LMS}} x_{\mathrm{in}}(n) \end{aligned} \tag{3}$$

where φ is the estimated phase and d is the detected symbol. In our simulation we observed up to 1-dB improvement in required OSNR for target BER $= 10^{-3}$ by switching to decision-directed mode.

Joint carrier recovery is done using feed-forward carrier recovery [21]. Note that optimized joint carrier phase recovery of a block of M subcarriers reduces the phase-error variance, permitting up to an M-fold increase in laser linewidth. Phase recovery is interleaved with equalizer adaptation, as shown in Fig. 5. The update interval of the decision-directed adaptive filter depends on the delay of the FIR filter used for phase recovery. Hence, there is a tradeoff between the accuracy of carrier phase estimation and the convergence time and tracking performance of the adaptive filter [20]. In our simulation we used a 21-symbol-long FIR filter for hard phase estimation, resulting in adaptive filter update interval of 10 symbols.

B. Sampling Rate and Multiple Carriers per Sampling

In order to be compatible with the recent ITU flexible grid standard [17] and available WSS technologies [22], the per-subcarrier symbol rate R_s should be a multiple of 12.5 GHz. On the other hand, NGI-OFDM requires an ADC with sampling rate $R_{\mathrm{samp}} \geq 4R_s$ to suppress XCI between subcarriers [15]. Since a prototype ADC with 32.5-GHz bandwidth and $R_{\mathrm{samp}} =$ 80 GSample/s prototype ADC has recently been demonstrated [23], we assume an ADC with $R_{\mathrm{samp}} = 75$ GSample/s and a symbol rate $R_s = 12.5$ GHz, corresponding to 6 samples per symbol.

With sampling rate $R_{\mathrm{samp}} = 75$ GHz, simultaneous detection of up to $M = 4$ subcarriers is possible, albeit with some penalty, as the Nyquist bandwidth is not sufficient to include all the interfering neighbors. Fig. 6 shows the bit-error ratio (BER) averaged over the M subcarriers detected in each receiver for a superchannel comprising 24 subcarriers, which conveys approximately 1.1 Tbit/s with a spectral efficiency of 3.5 bits/s/Hz. We observe a worst-case penalty of 1.1 dB at a target BER of 10^{-3} for a system with $M = 1$, as compared to detection of a single isolated subcarrier. We observe additional penalties of 0.7, 1.2 and 1.5 dB for detecting $M = 2$, 3 and 4 subcarriers per sampling, respectively. These penalties are smaller than the penalties reported in [18] mainly because of the higher sampling rate in our system. It can be observed in Fig. 6 that the subcarriers at the superchannel edges have better performance, as they have fewer interfering neighbors.

The power penalties have been obtained by Monte Carlo simulation of a superchannel consisting of 24 subcarriers, each with $2^{14}-1 = 16{,}383$ symbols generated by a linear feedback shift register with 14 taps. The system parameter values used in the simulation are typical of a dispersion-uncompensated long-haul system: $N_A = 40$ spans, $L_{\mathrm{SMF}} = 80$ km, $\alpha_{\mathrm{SMF}} =$ 0.25 dB/km, $D_{\mathrm{SMF}} = 17$ ps/nm·km, mean DGD of 4.5ps, and amplifiers with spontaneous emission factor $n_{\mathrm{sp}} = 1.58$ (noise figure $F_n = 5.0$ dB) with total gain compensating the total span loss.

C. Symbol Timing Synchronization

In order to maintain orthogonality between the subcarriers, symbol alignment of the modulated subcarriers is necessary. We assume that all transmit symbol clocks are locked to a common reference. To avoid clock skew, each transmitter applies a fixed de-skewing correction. The calibration can be done once the transmitters are plugged in and stored in a lookup table [11].

D. Phase and Frequency Synchronization

In an NGI-OFDM system, phase and frequency synchronization errors lead to ICI. In the presence of these errors, the received signal can be written as

$$\begin{aligned} r(t) = &\left[e^{j2\pi \Delta f_{Rx} t + j\theta_{Rx}(t)} \left(s(t) e^{j2\pi \Delta f_{Tx} t + j\theta_{Tx}(t)} * h_f(t) \right) \right] \\ &* h_{aa}(t) * h_e(t) \end{aligned} \tag{4}$$

where $h_f(t)$, $h_{aa}(t)$, and $h_e(t)$ are the impulse responses of the fiber, anti-aliasing filter, and FDE, respectively, Δf and θ are the frequency locking error and phase noise of the laser, and $s(t)$ is the transmitted waveform. For NGI-OFDM, $s(t)$ can be

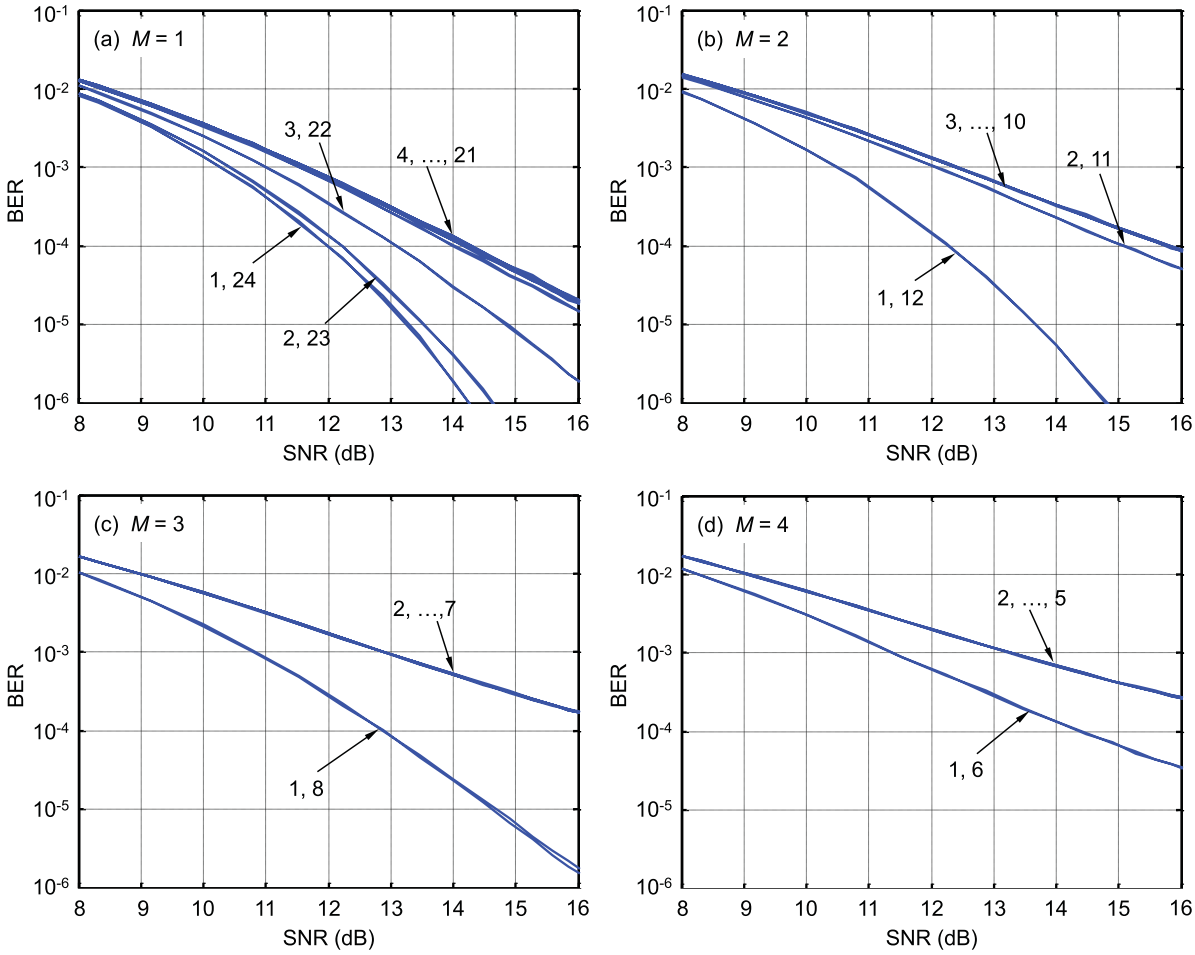

Fig. 6. Average bit-error ratio (BER) versus signal-to-noise ratio (SNR) for each transceiver detecting a 24-subcarrier superchannel. The numbers of subcarriers detected per transceiver are: (a) $M = 1$, (b) $M = 2$, (c) $M = 3$, (d) $M = 4$. The transceiver indices are indicated.

represented as

$$s(t) = \sum_{k=1}^{Nc} c_k \cdot s_k(t) \tag{5}$$

where c_k is the transmitted symbol of kth subcarrier, $N_c = N{\cdot}M$ is the total number of subcarriers, and $\{s_k\}$ is set of frequency-shifted rectangular pulses with duration of the symbol period T_s, given by

$$\begin{aligned} s_k(t) &= \Pi(t)e^{j2\pi f_k t}, \;\; 1 < k < N_c \\ \Pi(t) &= \begin{cases} 1, & 0 < t \le T_s \\ 0, & t \le 0, t > T_s \end{cases} \end{aligned} \tag{6}$$

which satisfy

$$f_k - f_j = \frac{k-j}{T_s}, 1 < k < N_c. \tag{7}$$

Our analysis of phase- and frequency-synchronization errors for NGI-OFDM generated by cooperative transceivers is similar to that in studies of DFT-based OFDM [24], [25], except in a few details. In most OFDM system studies, it is assumed that each channel has a very large number of subcarriers, which is not the case here. Moreover, in our design, different subcarriers may be generated by different lasers with independent phase noise processes, making the analysis slightly more complicated.

1) Local Oscillator Frequency Errors: Here, we analyze the effects of frequency offsets and phase noise separately. We assume that the local oscillator (LO) is locked to the desired frequency with the accuracy of Δf_{LO}. Neglecting transmitter frequency and phase errors, the received signal for detection of the jth subcarrier can be written as

$$r_j(t) = e^{j2\pi\Delta f_{\mathrm{LO}} t}\left(\sum_{k=1}^{Nc} c_k \cdot s_k(t) * h_f(t)\right) * h_{aa}(t) * h_e(t). \tag{8}$$

Assuming a small LO-frequency error ($2\pi\beta_2 LR_s{\cdot}\Delta f_{\mathrm{LO}} \ll 1$), which is true for typical long-haul systems, we can commute the frequency offset operation and $h_f(t)$. Hence

$$\begin{aligned} r_j(t) &\approx \sum_{k=1}^{Nc} c_k \cdot s_k(t)e^{j2\pi\Delta f_{\mathrm{LO}} t} * h_f(t) * h_{aa}(t) * h_e(t) \\ &= \sum_{k=1}^{Nc} c_k \cdot \Pi(t)e^{j2\pi(f_k+\Delta f_{\mathrm{LO}})t} * h_{aa}(t). \end{aligned} \tag{9}$$

In (9) we used the fact that $h_e(t)$ is designed to compensate the fiber impairments and ideally it reverses the effects of $h_f(t)$.

Due to short duration of the pulse-shaping function, we can further simplify the calculation by assuming

$$\Pi(t)e^{j2\pi(f_k+\Delta f_{\rm LO})t} * h_{aa}(t) \approx H_k \Pi(t) e^{j2\pi(f_k+\Delta f_{\rm LO})t} \quad (10)$$

where H_k is the Fourier transform of the anti-aliasing filter at a frequency $f_k + \Delta f_{\rm LO}$. As mentioned before, the subcarrier separation filter is matched to a single subcarrier, so the detected symbol is given by

$$c'_j \approx \sum_{k=1}^{N_c} c_k H_k \frac{1}{Ts} \int_0^{T_s} e^{j2\pi f_k t} \cdot e^{j2\pi(f_j+\Delta f_{\rm LO})t} \cdot dt$$

$$= \gamma_0 c_j + \sum_{\substack{k=1 \\ k \neq j}}^{N_c} H_k \gamma_{j-k} c_k \quad (11)$$

where

$$\gamma_k(\Delta f) = \frac{\sin(\pi \Delta f T_s)}{\pi(k - \Delta f T_s)} e^{-j\pi(k-\Delta f T_s)}. \quad (12)$$

In (15), the first term causes the detected symbols to be rotated and scaled by γ_0, and the second term introduces ICI with variance of

$$\sigma^2_{\rm ICI} = \sum_{\substack{k=1 \\ k \neq j}}^{N_c} \gamma^2_{k-j} |H_k|^2 P \quad (13)$$

where P is the power of each subcarrier. Assuming that the interference is Gaussian-distributed, the effective SNR of the jth subcarrier is given by

$$\text{SNR}_j \approx \frac{\gamma_0^2 P}{\sigma^2_{\rm AWGN} + \sigma^2_{\rm ICI}} \quad (14)$$

where $\sigma^2_{\rm AWGN}$ is the variance of additive white Gaussian noise introduce by the amplifiers. Assuming all subcarriers use polarization-multiplexed quadrature phase-shift keying, the BER of the jth subcarrier is given by [26]

$$P_b = Q\left(\sqrt{\text{SNR}_j}\right). \quad (15)$$

Note that $\arg(\gamma_0)$ is the same for all of the detected subcarriers within a block. For small frequency error, the common phase can be tracked by feed-forward carrier phase recovery, but for larger errors frequency estimation is required [20]. Here we are only interested in the effects of adjacent subcarriers and we assume perfect estimation of $\arg(\gamma_0)$. Fig. 7 shows the average BER of a superchannel in the presence of LO frequency-locking error with common phase correction. The ICI given by (13) is independent of M. Therefore, the system with $M = 1$ is more sensitive to LO frequency error, as it has the smallest required SNR for any target BER. In Fig. 7, we observe that the analytical approach is able to accurately estimate the SNR of each subcarrier.

2) Transmitter Frequency Errors: In the proposed system, all transmit lasers are frequency-locked to a frequency comb reference, as shown in Fig. 1. Such a comb can be generated by successive phase modulation of a seed laser in an amplified circulating loop [27], [28]. The absolute frequency accuracy of each transmit laser depends on the absolute accuracy of the seed, the frequency spacing accuracy, and the locking accuracy

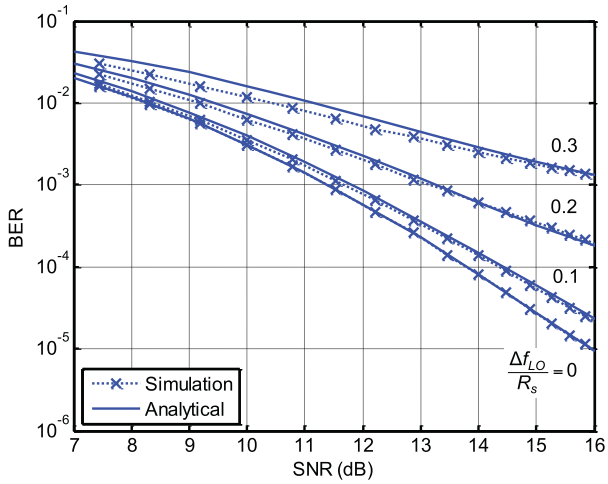

Fig. 7. Average BER versus SNR in the presence of LO frequency-locking error for $M = 1$. Frequency errors are normalized to the subcarrier spacing. BERs are averaged over a 24-subcarrier superchannel.

of each laser. The seed laser is assumed locked to an absolute frequency reference with an accuracy of order 1 GHz [28]. This error has a negligible impact, since all subcarriers within a superchannel share a common reference comb. The frequency spacing which, as mentioned before, is exactly matched to the symbol rate, is determined by the oscillator driving the phase modulator [27].

For typical crystal accuracy of 10–100 ppm [29] this error also has a negligible impact. The locking accuracy of individual transmit lasers is the dominant source of error, and can introduce interference on the desired subcarriers. The worst-case scenario happens when frequency errors push neighboring subcarriers toward the desired subcarrier. In this case, assuming the LO can be locked perfectly to the desired block for detection of the jth subcarrier, the received signal can be simplified to

$$r_j(t) = \left(\sum_{k=1}^{Nc} c_k \cdot s_k(t) e^{j2\pi\Delta f_{Tx}(k)t} * h_f(t)\right) * h_{aa}(t) * h_e(t) \quad (16)$$

where $|\Delta f_{Tx}(k)|$ is zero if j and k are generated by a same transceiver and Δf_{Tx} otherwise. Using a similar analysis as before, we can write the received signal as

$$r_j(t) \approx \sum_{k=1}^{Nc} c_k H_k \cdot \Pi(t) e^{j2\pi(f_k+\Delta f_{Tx}(k))t} \quad (17)$$

where H_k is the Fourier transform of the anti-aliasing filter at a frequency $f_k + \Delta f_{Tx}(k)$. The detected symbol is then given by

$$c'_j \approx \sum_{k=1}^{N_c} c_k H_k \frac{1}{Ts} \int_0^{T_s} e^{j2\pi f_k t} \cdot e^{j2\pi(f_j+\Delta f_{Tx}(k))t} \cdot dt$$

$$= c_j + \sum_{\substack{j,\, k \text{not} \\ \text{in same block}}} H_k \gamma_{|k-j|} c_k. \quad (18)$$

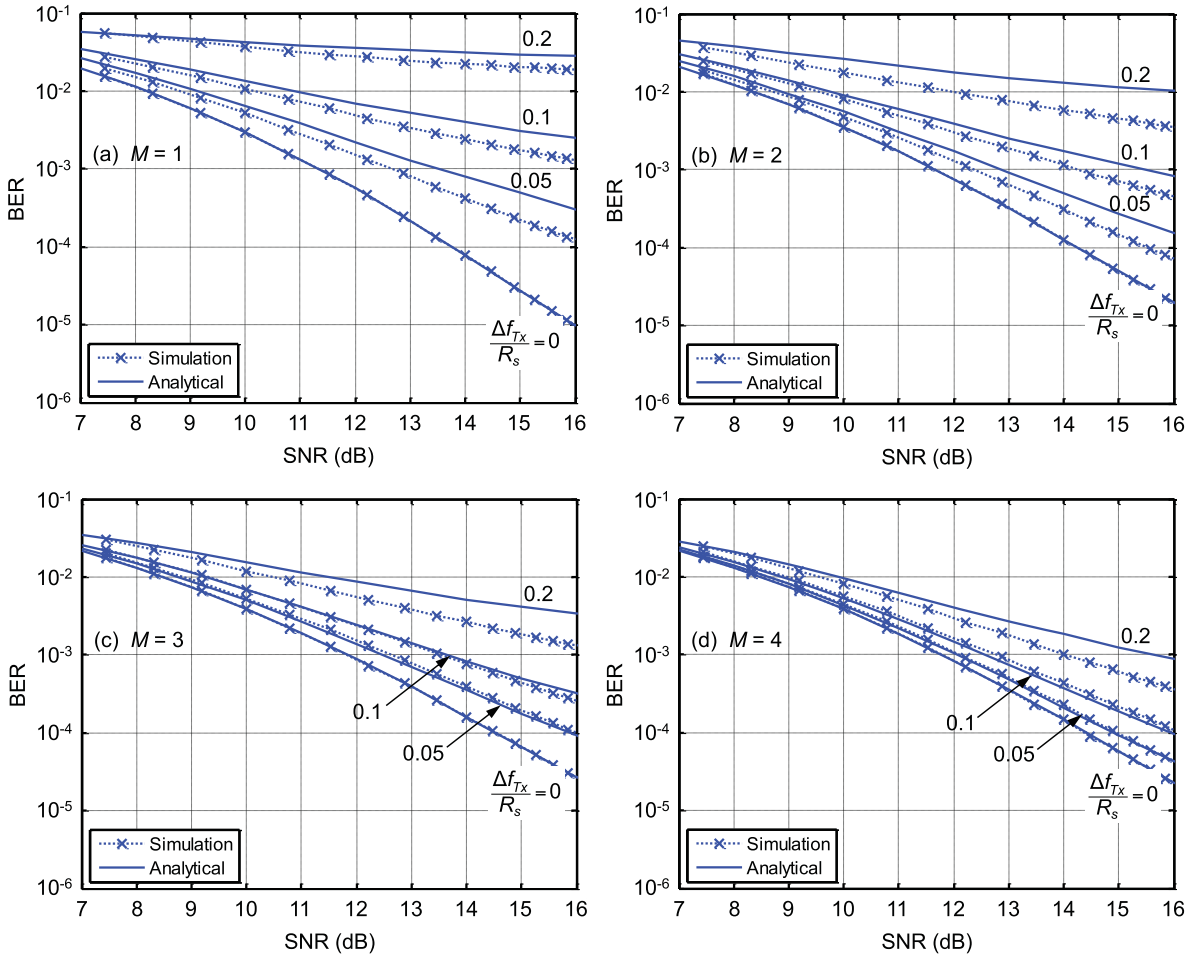

Fig. 8. Average BER versus SNR in the presence of frequency error in transmit lasers of the adjacent subcarriers for simultaneous detection of (a) $M = 1$, (b) $M = 2$, (c) $M = 3$, (d) $M = 4$ subcarriers. Frequency errors are normalized to the subcarrier spacing. BERs are averaged over a 24-subcarrier superchannel.

The second term in (12) is the ICI due to the frequency error, which has a variance

$$\sigma^2_{\mathrm{ICI}} = \sum_{\substack{j,k\mathrm{not} \\ \mathrm{insameblock}}} \gamma^2_{|k-j|} \left|H_k\right|^2 P. \tag{19}$$

Fig. 8 shows the average BER of the superchannel in the presence of the worst-case frequency error. We observe that the analytical approximation predicts the SNR with reasonable accuracy. The small gap between BERs computed analytically and obtained by simulation arises mainly because ICI is not Gaussian-distributed. In Fig. 8, the ICI penalty is largest for $M = 1$, as all of the interfering neighbors are generated by different lasers with different frequency errors. By comparing Fig. 7 to Fig. 8, we realize that the performance is more sensitive to transmit frequency locking than LO frequency locking. Assuming same locking errors for LO and transmit laser, accuracy of $\Delta f = 250$ MHz is required to have total penalty of 0.5 dB at target BER of 10^{-3} for $M = 1$.

3) Phase Noise: We now analyze the effects of laser phase noise on the performance of the proposed architecture and discuss laser linewidth requirements. We assume the laser phase fluctuations can be modeled as a Wiener process with zero mean and independent Gaussian increments with variance $\sigma^2(\Delta t) = 2\pi\beta\Delta t$, where β is the laser linewidth. Laser phase noise causes two major effects: (i) phase error in the detected subcarriers and (ii) ICI due to the phase fluctuations of adjacent subcarriers.

Feed-forward carrier phase recovery is employed to estimate the carrier phase of the desired subcarrier. In [21], transmitter and LO linewidth requirements for QAM were studied for the regime in which the CD is negligible. In [30], it was shown that significant uncompensated CD can lead to equalization-enhanced phase noise (EEPN), further restricting the linewidth of the LO. The impact of EEPN can be evaluated in terms of its additional SNR penalty. The effective SNR in the presence of EEPN is given by [30]

$$\mathrm{SNR_j} \approx \frac{P\left(1-\sigma^2_{\mathrm{T}}\right)}{P\sigma^2_T + \sigma^2_{\mathrm{AWGN}}} \tag{20}$$

where σ^2_T is the total interference, given by

$$\sigma^2_T = \pi c \left(2f_0^2\right)^{-1} D_t R_s \beta \tag{21}$$

where f_0 is the laser center frequency and D_t is the accumulated chromatic dispersion.

In addition to the phase error of the detected symbols, the phase fluctuations of adjacent subcarriers over a symbol period results in a loss of orthogonality, causing ICI. In the absence of

frequency offset and assuming perfect phase recovery, using the same analysis as before, the received signal can be simplified as

$$r_j(t) \approx \sum_{k=1}^{Nc} c_k \cdot s_k(t) e^{j(\theta_{Rx}(t)+\theta_{Tx}(t,k))} * h_{aa}(t) \tag{22}$$

where $\{\theta_{Tx}(t, k)\}$ is set of independent, identically distributed Weiner processes describing the phase fluctuation of different lasers. Assuming identical linewidths for the transmitter and LO lasers, $\theta_{Rx}(t) + \theta_{Tx}(t, k)$ can be modeled as a Weiner process $\theta(t)$ with variance of $\sigma^2(\Delta t) = 4\pi\beta\Delta t$. We note that the above simplification is valid only for systems with small accumulated dispersion. The detected symbol of the jth subcarrier is given by

$$c_j' \approx \eta_0 c_j + \sum_{\substack{k=1 \\ k\neq j}}^{N_c} H_k \eta_{j-k} c_k \tag{23}$$

where

$$\eta_k = \frac{1}{T_s} \int_0^{T_s} e^{j\left(\frac{2\pi k t}{T_s} + \theta(t)\right)} dt. \tag{24}$$

Assuming the receiver can perfectly estimate the $\varphi = \arg(\eta_0)$,

$$c_j' e^{-j\phi} \approx |\eta_0|\, c_j + e^{-j\phi} \sum_{\substack{k=1 \\ k\neq j}}^{N_c} H_k \eta_{j-k} c_k. \tag{25}$$

Expressing $|\eta_0| = \Delta + \delta$ with $\Delta = E[|\eta_0|]$, the effective SNR is given by [24]

$$\mathrm{SNR}_j \approx \frac{\Delta^2 P}{\sigma^2_{\mathrm{AWGN}} + \sigma^2_{\mathrm{ICI}}} \tag{26}$$

where the variance of ICI is

$$\sigma^2_{\mathrm{ICI}} = E[|\delta|^2] + \sum_{\substack{k=1 \\ k\neq j}}^{N_c} E[\eta^2_{k-j}] \cdot |H_k|^2 P \tag{27}$$

Using similar approximations as in [24] for small impairments, the ICI variance is bounded by

$$\sigma^2_{\mathrm{ICI}} \leq E[|\delta|^2] + |H_0|^2 P \left(1 - E[\eta_0^2]\right). \tag{28}$$

Fig. 9 shows the additional required SNR penalty at target BER of 10^{-3} due to ICI. It can be seen that linewidth requirements are dominated by EEPN, and ICI has a negligible impact. Note that the interference due to the EEPN is proportional to the accumulated dispersion and hence proportional to the fiber length. In Fig. 9, the SNR penalty is calculated after 3200 km of fiber, which is in the range of terrestrial long-haul deployments.

In Fig. 10, the total SNR penalty due to the phase noise is shown for different values of M. Per-laser linewidths of 350 and 500 kHz are required for $M = 1$ and $M = 4$, respectively for 0.5-dB penalty. All of the above linewidth requirements can be met using commercially available lasers [31].

IV. Conclusion

We proposed a modular architecture supporting variable-bandwidth superchannels for future long-haul optical networks.

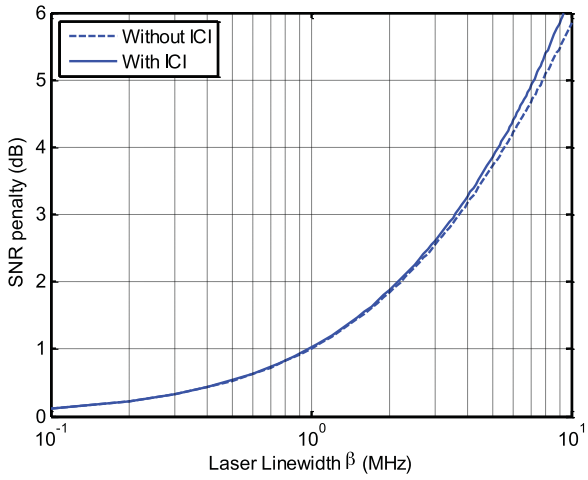

Fig. 9. Worst-case SNR penalty due to phase noise versus laser linewidth for $M = 1$ at 10^{-3} target BER. The solid and dashed lines show the penalties calculated with and without inter-subcarrier interference.

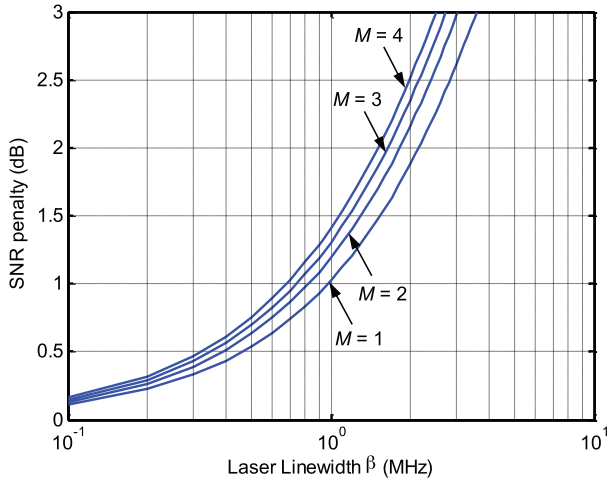

Fig. 10. Worst-case total SNR penalty at 10^{-3} target BER for simultaneous detection of M subcarriers for $M = 1, 2, 3, 4$.

This architecture, in principle, can be implemented using either NGI-OFDM or DFT-based OFDM. Using NGI-OFDM, the architecture achieves the same flexibility as Nyquist-WDM, but with higher spectral efficiency. In particular, the proposed network can be designed to support bit rates scalable from 50 Gbit/s to beyond 1 Tbit/s using available technologies. The proposed architecture employs colorless transceivers. Each transceiver can operate individually to transmit/receive up to $M = 4$ subcarriers with symbol rates of 12.5 GHz. A set of N transceivers can cooperate to transmit/receive a superchannel comprising $N{\cdot}M$ subcarriers, each conveying up to 200 Gbit/s. The synchronization is required between transmitters and there is no cooperation between receivers. Future work should address cooperation between receivers to compensate linear ICI and nonlinear effects such as XPM between subcarriers.

We analyzed and simulated NGI-OFDM implementations of the architecture and the impact of various impairments, including fiber dispersion, aliasing, and carrier phase and frequency errors. We studied the performance of transceivers modulating/

detecting M subcarriers simultaneously. While a system with $M = 1$ has a better performance, systems with higher M are more cost efficient and less sensitive to frequency errors.

We also described possible realizations of gapless (de)multiplexers for variable-bandwidth superchannels. While a dual-mode WSS minimizes optical power loss, a conventional WSS combined with power splitters provides more scalability.

ACKNOWLEDGMENT

The authors would like to thank L. Beygi for helpful discussions and suggestions.

REFERENCES

[1] A. Sano, E. Yamada, H. Masuda, E. Yamazaki, T. Kobayashi, E. Yoshida, Y. Miyamoto, R. Kudo, K. Ishihara, and Y. Takatori, "No-guard-interval coherent optical OFDM for 100-Gb/s long-haul WDM transmission," *J. Lightw. Technol.*, vol. 27, no. 16, pp. 3705–3713, Aug. 2009.

[2] S. Chandrasekhar and X. Liu, "Terabit superchannels for high spectral efficiency transmission," presented at the Eur. Conf. Exhib. Opt. Commun., Torino, Italy, 2010.

[3] B. Zhu, X. Liu, S. Chandrasekhar, D. W. Peckham, and R. Lingle, "Ultra-long-haul transmission of 1.2-Tb/s multicarrier no-guard-interval CO-OFDM superchannel using ultra-large-area fiber," *IEEE Photon. Technol. Lett.*, vol. 22, no. 11, pp. 826–828, Jun. 2010.

[4] J. Yu *et al.*, "Generation, transmission and coherent detection of 11.2 Tb/s (112×100 Gb/s) single source optical OFDM superchannel," presented at the Opt. Fiber Commun. Conf., Los Angeles, CA, USA, 2011, Paper PDPA6.

[5] G. Bosco, V. Curri, A. Carena, P. Poggiolini, and F. Forghieri, "On the performance of Nyquist-WDM terabit superchannels based on PM-BPSK, PM-QPSK, PM-8QAM or PM-16QAM subcarriers," *J. Lightw. Technol.*, vol. 29, no. 1, pp. 53–61, Jan. 2011.

[6] G. Gavioli, E. Torrengo, G. Bosco, A. Carena, S. J. Savory, F. Forghieri, and P. Poggiolini, "Ultra-narrow-spacing 10-channel 1.12 Tb/s D-WDM long-haul transmission over uncompensated SMF and NZDSF," *IEEE Photon. Technol. Lett.*, vol. 22, no. 19, pp. 1419–1421, Oct. 2010.

[7] G. Bosco, A. Carena, V. Curri, P. Poggiolini, and F. Forghieri, "Performance limits of nyquist-WDM and CO-OFDM in high-speed PM-QPSK systems," *IEEE Photon. Technol. Lett.*, vol. 22, no. 15, pp. 1129–1131, Aug. 2010.

[8] M. Yan, Z. Tao, W. Yan, L. Li, T. Hoshida, and J. C. Rasmussen, "Experimental comparison of no-guard-interval-OFDM and nyquist WDM superchannels," presented at the Opt. Fiber Commun. Conf., Los Angeles, CA, USA, 2010.

[9] R. Dischler and F. Buchali, "Transmission of 1.2 Tb/s continuous waveband PDM-OFDM-FDM signal with spectral efficiency of 3.3 bit/s/Hz over 400 km of SSMF," in *presented at the Opt. Fiber Commun. Conf.*, San Diego, CA, USA, 2009, Paper PDPC2.

[10] Y. Ma, Q. Yang, Y. Tang, S. Chen, and W. Shieh, "1-Tb/s single-channel coherent optical OFDM transmission over 600-km SSMF fiber with subwavelength bandwidth access," *Opt. Exp.*, vol. 17, no. 11, pp. 9421–9427, 2009.

[11] D. J. F. Barros, J. M. Kahn, T. A. Z. Jeffrey, and P. Wilde, "Bandwidth-scalable long-haul transmission using synchronized colorless transceivers and efficient wavelength-selective switches," *J. Lightw. Technol.*, vol. 30, no. 16, pp. 2646–2660, Aug. 2012.

[12] E. Ip and J. M. Kahn, "Fiber impairment compensation using coherent detection and digital signal processing," *J. Lightw. Technol.*, vol. 28, no. 4, pp. 502–519, Feb. 2010.

[13] J. Schroder, L. B. Du, M. M. Morshed, B. J. Eggleton, and A. J. Lowery, "Colorless flexible signal generator for elastic networks and rapid prototyping," presented at the Opt. Fiber Commun. Conf., Anaheim, CA, USA, 2013.

[14] D. J. F. Barros and J. M. Kahn, "Optical modulator optimization for orthogonal frequency-division multiplexing," *J. Lightw. Technol.*, vol. 27, no. 13, pp. 2370–2378, Jul. 2009.

[15] S. Chandrasekhar and X. Liu, "Experimental investigation on the performance of closely spaced multi-carrier PDM-QPSK with digital coherent detection," *Opt. Exp.*, vol. 17, no. 24, pp. 21350–21361, 2009.

[16] M. D. Feuer, D. C. Kilper, and S. L. Woodward, "ROADMs and their system applications," in *Optical Fiber Telecommunications V-B*. New York, NY, USA: Academic, 2008.

[17] Spectral grids for WDM applications: DWDM frequency grid, I.-T. G.694.1, 2012.

[18] X. Liu, S. Chandrasekhar, B. Zhu, and D. Peckham, "Efficient digital coherent detection of A 1.2-Tb/s 24-carrier no-guard-interval CO-OFDM signal by simultaneously detecting multiple carriers per sampling," presented at the Opt. Fiber Commun Conf., San Diego, CA, USA, 2010.

[19] T. Kobayashi, R. Kudo, Y. Takatori, A. Sano, E. Yamada, H. Masuda, M. Matsui, M. Mizoguchi, and Y. Miyamoto, "Frequency-domain equalisation without guard interval for optical transmission systems," *Electron. Lett.*, vol. 44, no. 25, pp. 1480–1482, 2008.

[20] S. J. Savory, "Digital filters for coherent optical receivers," *Opt. Exp.*, vol. 16, no. 2, pp. 804–817, 2008.

[21] E. Ip and J. Kahn, "Feedforward carrier recovery for coherent optical communications," *J. Lightw. Technol.*, vol. 25, no. 9, pp. 2675–2692, Sep. 2007.

[22] S. Frisken, S. Poole, and G. Baxter, "Wavelength-selective reconfiguration in transparent agile optical networks," *Proc. IEEE*, vol. 100, no. 5, pp. 1056–1064, May 2012.

[23] X. Liu, S. Chandrasekhar, P. Winzer, B. Zhu, D. Peckham, S. Draving, J. Evangelista, N. Hoffman, C. Youn, Y. Kwon, and E. Nam, "3 × 485-Gb/s WDM transmission over 4800 km of ULAF and 12 × 100-GHz WSSs using CO-OFDM and single coherent detection with 80-GS/s ADCs," presented at the Opt. Fiber Commun. Conf., Los Angeles, CA, USA, 2011.

[24] T. Pollet, M. Van Bladel, and M. Moeneclaey, "BER sensitivity of OFDM systems to carrier frequency offset and Wiener phase noise," *IEEE Trans. Commun.*, vol. 43, no. 234, pp. 191–193, Feb./Mar./Apr. 1995.

[25] W. Shieh, "OFDM for flexible high-speed optical networks," *J. Lightw. Technol.*, vol. 29, no. 10, pp. 1560–1577, May 2011.

[26] J. G. Proakis, *Digital Communications*, 4th ed. New York, NY, USA: McGraw-Hill, 2002.

[27] K. P. Ho and J. M. Kahn, "Optical frequency comb generator using phase modulation in amplified circulating loop," *IEEE Photon. Technol. Lett.*, vol. 5, no. 6, p. 721—725, Jun. 1993.

[28] S. Bennett, B. Cai, E. Burr, O. Gough, and A. J. Seeds, "1.8-THz bandwidth, zero-frequency error, tunable optical comb generator for DWDM applications," *IEEE Photon. Technol. Lett.*, vol. 11, no. 5, pp. 551–553, May 1999.

[29] A. Chenakin, *Frequency Synthesizers: Concept to Product*. Norwood, MA, USA: Artech House, 2011.

[30] W. Shieh and K. P. Ho, "Equalization-enhanced phase noise for coherent-detection systems using electronic digital signal processing," *Opt. Exp.*, vol. 16, no. 20, pp. 15718–15727, 2008.

[31] J. P. Wilde, G. W. Yoffe, and J. M. Kahn, "Frequency noise characterization of a widely tunable narrow-linewidth DFB laser array source," presented at the Opt. Fiber Commun. Conf., San Diego, CA, USA, 2009.

Milad Sharif received the B.S. degree in electrical engineering from the Sharif University of Technology, Tehran, Iran, in 2010, and the M.S. degree in electrical engineering from Stanford University, Stanford, CA, USA, in 2012, where he is currently working toward the Ph.D. degree in electrical engineering.

His current research interests include long-haul optical networks and associated digital signal processing, optical interconnects for data centers, and optical access networks.

Joseph M. Kahn (M'90–SM'98–F'00) received the A.B., M.A., and Ph.D. degrees in physics from University of California, Berkeley (UC Berkeley), Berkeley, CA, USA, in 1981, 1983, and 1986, respectively.

From 1987–1990, he was with AT&T Bell Laboratories, Crawford Hill Laboratory, Holmdel, NJ, USA. He demonstrated multi-Gbit/s coherent optical fiber transmission systems, setting world records for receiver sensitivity. From 1990–2003, he was on the Faculty of the Department of Electrical Engineering and Computer Sciences at UC Berkeley, performing research on optical and wireless communications. Since 2003, he has been a Professor of electrical engineering at Stanford University, Stanford, CA, USA, where he heads the Optical Communications Group. His current research interests include: fiber-based imaging, spatial multiplexing, rate-adaptive and spectrally efficient modulation and coding methods, coherent detection and associated digital signal processing algorithms, digital compensation of fiber nonlinearity, and free-space systems. In 2000, he helped found StrataLight Communications, where he served as a Chief Scientist from 2000–2003. StrataLight was acquired by Opnext, Inc. in 2009.

Prof. Kahn received the National Science Foundation Presidential Young Investigator Award in 1991. From 1993–2000, he served as a Technical Editor of IEEE *Personal Communications Magazine*. Since 2009, he has been an Associate Editor of IEEE/OSA *Journal of Optical Communications and Networking*.